Land Displacement Mapping of Eastern Nepal using DInSAR Technique and Sentinel-1 data

Shweta Sharma, Y.S. Rao* and A.K. Mathur

***Indian Institute of Technology Bombay, Mumbai**

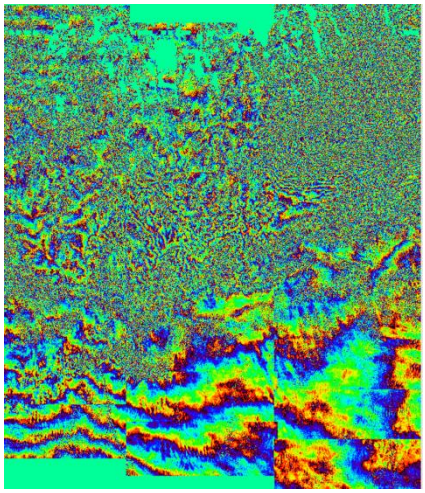

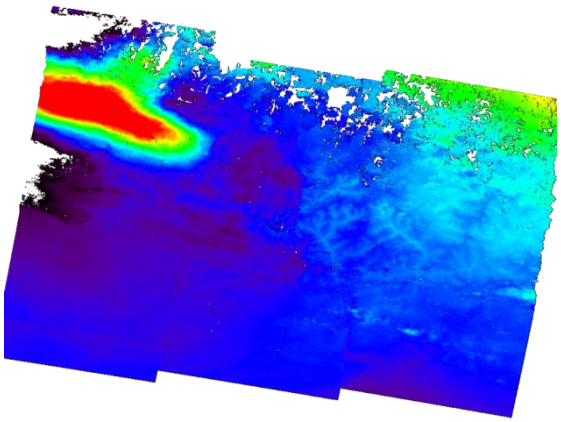

Calibration and Validation Division
Atmosphere & Ocean Data Validation, Archival and Dissemination Group
Earth, Ocean, Atmosphere, Planetary Sciences & Applications Area
Space Applications Centre,
ISRO, Ahmedabad

MAY 2015

Abstract

The capital city of Nepal and surrounding areas was hit by 7.8 magnitude on 25th April 2015 followed by large number of aftershocks including 7.3 magnitude earthquake on 12th May 2015 respectively. The epicenter of first earthquake was the village of Barpak, Gorkha district, and its hypocenter was at a depth of approximately 15 km (source:Wikipedia). The epicenter of the second one was near the Chinese border between the capital of Kathmandu and Mt. Everest. To study the deformation due to this earthquake event, in this work, differential synthetic aperture radar interferometry (DInSAR) technique has been used. This technique has already proven its capacity for variety of applications including ground deformation mapping. With the launch of Sentinel-1A on April 2014 and release of its data on May 2015, numerous services have been benefitted including the monitoring of land-surface for motion risks, mapping for forest, water and soil management and mapping to support humanitarian aid and crisis situations. In the present study, using Sentinel-1 data and SRTM 90m and SRTM 30m DEM deformation maps were obtained for eastern part of Nepal. The results shows the deformation in the range of -37.5 cm to 93.5 cm with the mean standard deviation of 10.5 cm for SRTM 90m DEM. The north-west part of the study area (near Kathmandu) shows the uplift that goes upto around 1 m, whereas the north-east part shows the uplift in the range of 11.5 cm to 68.9 cm. Southern part of the study area shows subsidence. By using SRTM 30 m DEM for a small part of far eastern Nepal the displacement range was found to be 31.1 cm to 1.78 m with mean standard deviation of 22.3. The refinement of the land displacement map using 1-arc second SRTM Data is in progress.

1.0 Introduction

The April 2015 earthquake (also known as Gorkha earthquake) occurred at 11:56 NST on 25 April, with a magnitude of 7.8 and epicenter in the village of Barpak, Gorkha district with hypocenter at a depth of approximately 15 km. The earthquake was followed by continued aftershocks with second major earthquake of magnitude 7.3 in Nepal on 12 May 2015 at 12:50 pm, 18 km southeast of Kodari at a depth of 18.5 kilometres. Its epicenter was on the border of Dolakha and Sindhupalchowk districts of Nepal. This earthquake occurred on the same fault as the larger magnitude 7.8 earthquake of 25 April, but further east than the original quake. The effect of this earthquake was so strong that the shaking was felt in northern parts of India also including Bihar, Uttar Pradesh and West Bengal. Figure 1 shows the map of Nepal along with the location of epicentre.

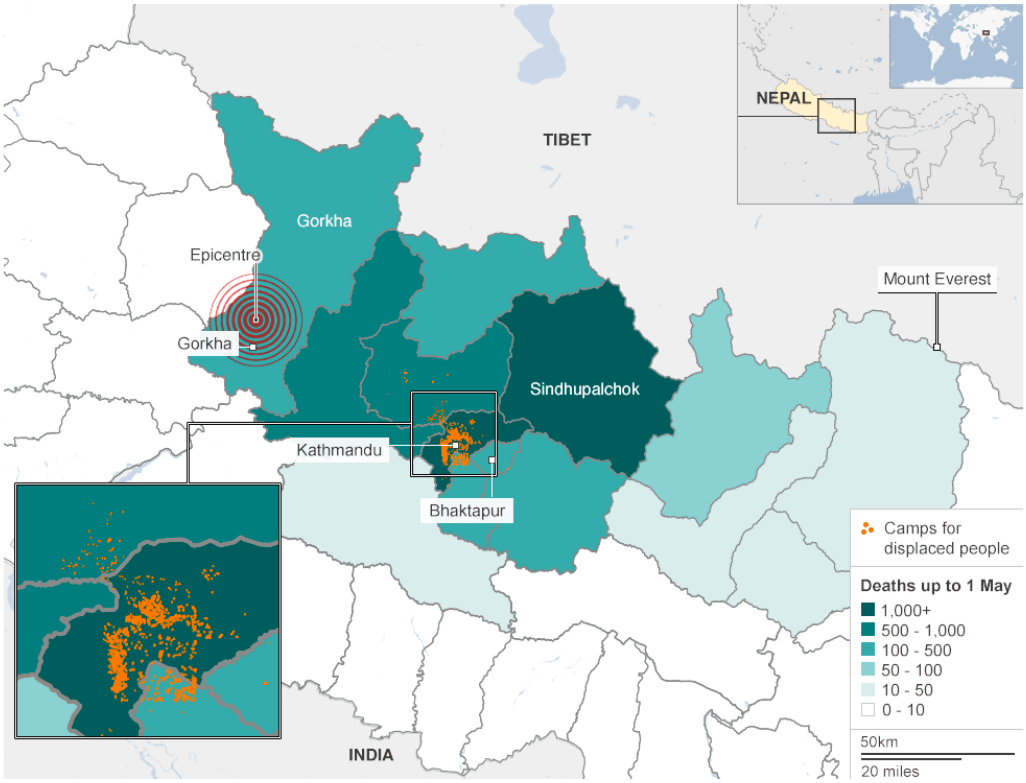

Figure 1: Map of Nepal showing the location of epicentre of Gorkha Earthquake

(Source: NGA, Nepalese government)

As the environmental and economic impacts of the land deformation events like earthquake, landslides etc. are very serious, it is very important to install the precise monitoring systems to monitor and observe the land surface movement. Traditionally, it is done by installing the discrete network of benchmarks and precisely levelling periodically. But with the advent of modern technologies like Global Positioning Systems (GPS), lately, GPS stations have been used, providing a relatively cheap and accurate measure of land deformation. Both methods allows the precise monitoring of land subsidence at the selected grid of points, but for large areas, the technique is time consuming and expensive (web1). Also, information on large areas is result of interpolation and shows inaccuracies. Also, these methods are not useful for the inaccessible locations (Raucoules et al., 2007). Because of the disadvantages of the conventional methods like GPS, levelling, total station, and extensometers for monitoring the ground surface movements; Spaceborne Radar Interferometry is used for regional-scale land deformation measurements and is popular because of the rapid and easily updatable acquisitions of data over wide areas that helps to reduce both field work and costs (web2). For the mapping and monitoring land deformation, DInSAR technique has been used

worldwide for the land deformation mapping and monitoring. In this work also DInSAR technique was used for mapping the land deformation caused due to the Gorkha earthquake in eastern Nepal and first cut results are reported.

2.0 Study Area and Data used

2.1 Study Area

Eastern part of the Nepal has been taken as the study area for this study (Figure 2). Nepal lies completely within the collision zone of Indian subcontinent and the Eurasian continent which produced the Himalaya and the Tibetan Plateau. Nepal occupies the central sector of the Himalayan arc (Pandey et al., 1999).

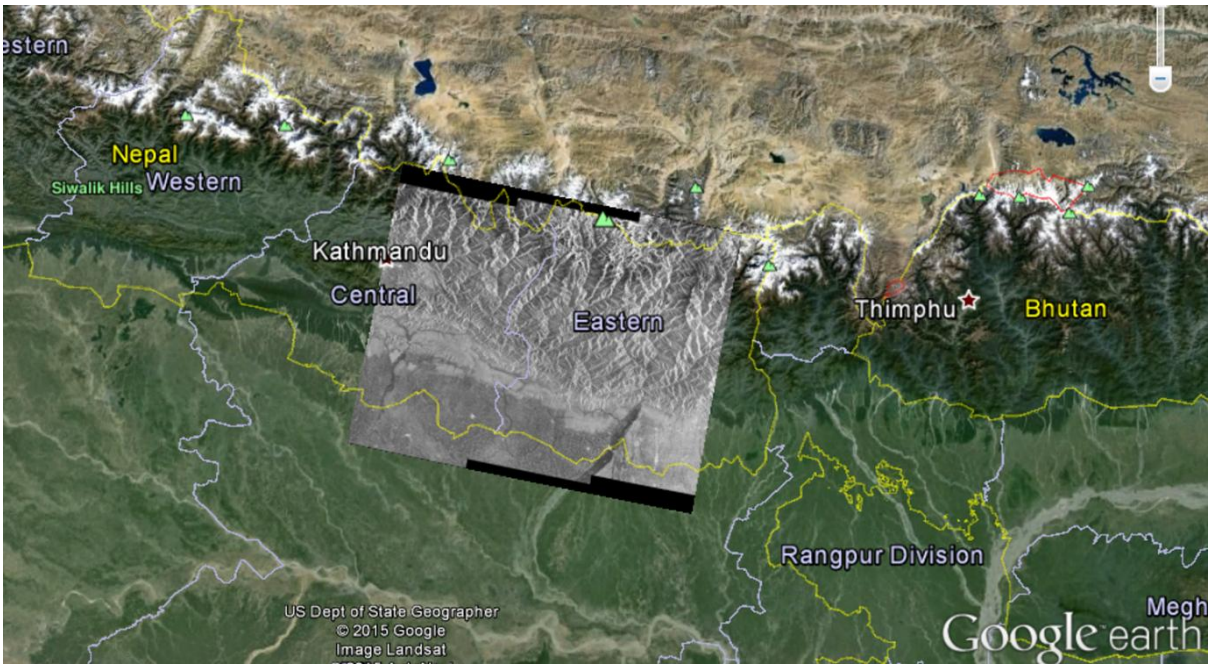

Figure 2: Study area overlaid on the Google Earth map (Courtesy: Google Earth)

It was shown in a study that the Indian plate continues to move north relative to Asia at the rate of approximately 50 mm per year (Bilham et al., 1994; Pandey et al., 1999). As the strong Indian continental crust subducts beneath the relatively weak Tibetan crust, it pushes up the Himalayan Mountains. This collision zone has accommodated huge amounts of crustal shortening as the rock sequences slide one over another. A study from 2015 (BBC, 2015) found a 700-year delay between earthquakes in the region. The study also suggests, that because of tectonic stress transfer, the earthquake from 1934 in Nepal and the 2015 earthquake are connected - following a historic earthquake pattern.

2.2 Data Used

Sentinel-1s radar can operate in four modes: Interferometric Wide swath (IW), Extra Wide Swath (EW), Wave (WV) and Stripmap (SM). In this study Sentinel-1, Interferometric Wide Swath SLC (IW-SLC), VV polarization data of 24th April 2015 and 6th May 2015 is used. Sentinel-1 is a space mission from ESA of the Copernicus Programme, consisting of a constellation of two satellites. The payload of Sentinel-1 is a Synthetic Aperture Radar in C-band that provides continuous imagery (day, night and all weather). Sentinel-1A was launched on 3 April 2014 on a Soyuz rocket from Europe's Spaceport in French Guiana. The Sentinel-1 satellites are expected to make analysis of earthquakes using InSAR techniques quicker and simpler.

IW SLCs, having three swaths, have three images in single polarisation and six images for dual polarisation. For IW, each sub-swath consists of a series of bursts. Each burst has been processed as a separate SLC image. The individually focused complex burst images are included, in azimuth-time order, into a single sub-swath image, with black-fill demarcation in between, similar to the ENVISAT ASAR Wide ScanSAR SLC products. For IW, a focused burst has a duration of 2.75 seconds and a burst overlap of approximately 50-100 samples.

Images for all bursts in all sub-swaths of an IW SLC product are re-sampled to a common pixel spacing grid in range and azimuth. Burst synchronization is ensured IW product. Unlike ASAR WSS, which contains a large overlap between beams, for SENTINEL-1 TOPSAR products, the imaged ground area of adjacent bursts only marginally overlap in azimuth just enough to provide contiguous coverage of the ground. This is due to the one natural azimuth look inherent in the data. Table-1 shows the properties that are particular to each sub-swath of the IW mode. Table-2 shows the properties that are common to all sub-swaths of the IW mode:

Table 1: Details of each sub-swath of the IW mode

Beam ID	IW1	IW2	IW3
Resolution rg x az m	2.7x21.7	3.1x21.7	3.5x21.6
Pixel spacing rg x az m	2.3x14.1	2.3x14.1	2.3x14.1
Incidence angle °	32.9	38.3	43.1
Range look bandwidth Hz	56.5	48.3	42.8
Azimuth look bandwidth Hz	327	313	314
Range Hamming weighting coefficient	0.75	0.75	0.75
Azimuth Hamming weighting coefficient	0.7	0.75	0.75

Table 1: Properties common to all sub-swaths of the IW mode

Product ID	IW_SLC
Pixel value	Complex
Coordinate system	Slant range
Bits per pixel	16 I and 16 Q
Polarisation options	Single (HH or VV) or Dual (HH+HV or VV+VH)
Ground range coverage km	251.8
Equivalent Number of Looks (ENL)	1
Radiometric resolution	3
Absolute location accuracy m (NRT)	7
Number of looks (range x azimuth)	1 x 1

For subtraction of the topography, SRTM 90m and SRTM 30 m DEM is used. A 1-arc second global digital elevation model (30 meters) (SRTM 30m DEM) has been released by United States Government at the end of the year 2014.

3.0 Theoretical Background

Interferometric SAR also referred to as SAR interferometry is the measurement of signal phase change or interference over time. InSAR utilizes the phase information of the images to extract useful geodetic information such as the height of the terrain, ground deformation etc.

Conventional Synthetic Aperture Radar interferometry (InSAR) deals with the pixel-by-pixel phase difference of two acquisitions, gathered at different times with slightly different looking angles. Spaceborne SAR interferometry has already proven a remarkable potential for two particular applications (of course among numerous others):

• The reconstruction of topographic digital elevation models (DEM) starting from interferometric pairs acquired from slightly different viewing angles (the different acquisition geometry is parameterized by normal baseline).

• The detection of surface deformation phenomena (e.g. volcano, co-seismic and post-seismic displacements along active faults as well as slope instability) starting from pairs spanning a convenient time interval. The deformation only in the line-of-sight of the sensor is obtained from the interferometric measurements.

Radar signals are characterized by a certain frequency of operation and for interferometric applications, they can be thought of as sinusoidal waves, one complete cycle from $-\pi$ to $+\pi$ corresponding to the wavelength. It is this specific property of the radar signal and the system's ability to record both amplitude and phase information for each image pixel that is used in estimating displacement. When a point on the ground moves, the distance between

the sensor and the point on the ground also changes and so the phase value recorded by a SAR sensor flying along a fixed obit will be affected too. The change in signal phase (ΔΦ) can be expressed in the form of following equation:

$$\Delta\varphi = \frac{4\pi}{\lambda}\Delta R + \alpha + \Delta\Phi_{scat}$$

Where λ is the wavelength, ΔR is the displacement and α is the phase shift due to different atmospheric conditions at the time of the two radar acquisitions; $\Delta\Phi_{scat}$ is the phase difference due to the change in the contribution from the scattering resolution cell. As a consequence any displacement of a radar target along the satellite line of sight creates a phase shift in the radar signal that can be detected by comparing the phase values of two SAR images acquired at different times.

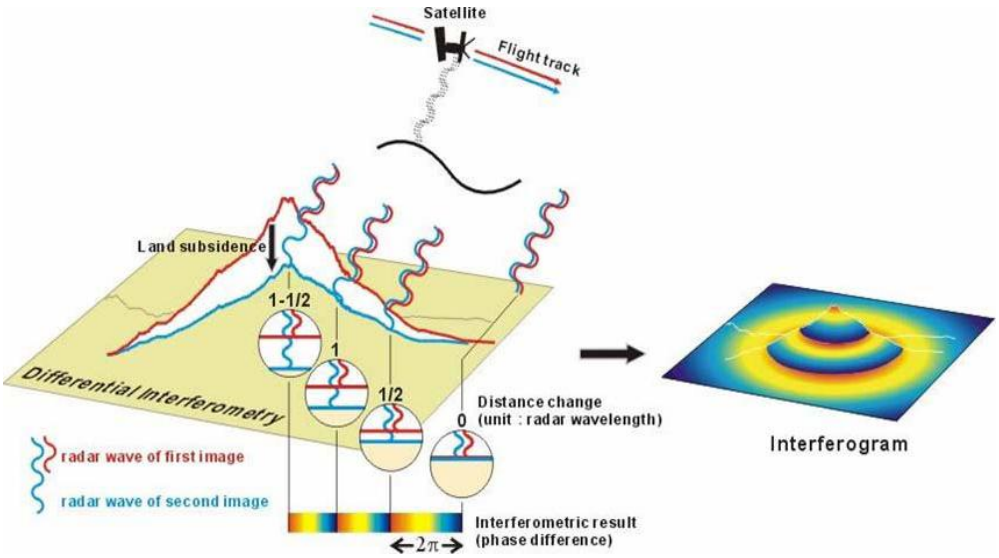

Figure 3: Principle for land deformation measurement

(Source:Chang et al. 2004)

But in order to use this method, following conditions should be met:

1. Images have to be acquired by the same satellite using the same acquisition mode and properties (beam, polarization, off-nadir angle etc.)
2. Images have to be acquired with the satellite in the same nominal orbit.
3. The baseline separation between the master scene and any of the slave scenes must be ideally zero for the deformation measurement, in contradictory to the case of DEM generation where the baseline separation should be no more than the critical baseline (a parameter that varies with the SAR sensor in use), the baseline being the distance between the satellite paths. This condition should be met so that the phase contribution because of the topography can be eliminated.

4. The scattering characteristics of the resolution cell should be the same for the two acquisitions so that the phase contribution from the changing scattering characteristics becomes zero.

Ignoring any phase shift due to atmospheric conditions and no change in the scattering characteristics of the targets in the same resolution cell, the estimated interferometric phase can be directly related to the difference in path length to a target from the imaging platform in the line of sight direction (Figure 3).

Differential Interferometry

Differential interferometry aims at the measurement of ground deformation using repeat-pass interferometry. Since line-of-sight displacements enter directly into the interferogram, independent of the baseline, it can be measured as a fraction of the wavelength. Unfortunately, non-zero baselines will always cause some sensitivity with respect to topography in the interferogram. The length of the perpendicular baseline deviates from zero since

1. It is often not possible- or not-desirable- to maneuver the satellite in a zero baseline orbit and
2. The baseline varies with the look angle, yielding only one zero-baseline range-bin in the interferogram.

The interferometric phase observation per resolution cell is composed by a number of contributors (Henssen, 2001)

$$\emptyset = 2\pi k + \phi_{topo} + \phi_{defo} + \phi_{orb} + \phi_{atm} + \phi_{scat} + \phi_{noise}$$

$$= 2\pi k + \frac{4\pi B_{\perp}}{\lambda R sin(\theta)} H + \frac{4\pi D}{\lambda} + \phi_{orb} + \phi_{atm} + \phi_{scat} + \phi_{noise}$$

The first term on the right hand side denotes the unknown integer number of full phase cycles or *phase ambiguity*. The topographic phase ϕ_{topo} is a function of the perpendicular baseline$B_{\perp}$, the look angle for the master platform θ and the slant range from the master platform to the Earth's surface R. It describes the height H above the reference surface. Further ϕ_{defo} is due to deformation D in the radar line-of-sight and ϕ_{orb} comprise the deterministic flat Earth component and the residual signal due to orbit errors. This residual signal forms a linear trend in the interferogram and can be estimated and removed beforehand. Alternatively it can be included in the atmospheric delayϕ_{atm}, because the atmosphere causes a linear trend as well. Either way, after removal of the flat earth component, the ϕ_{orb} term vanishes. The signal due to a change in the scatter characteristics

of the Earth's surface between the two observation times is denoted byϕ_{scat}. Finally, ϕ_{noise} represents the remaining noise terms, caused by for e.g. thermal noise, co-registration errors and interpolation errors.

For topographic mapping only ϕ_{topo} is the term of interest, whereas for land deformation studies, we want to extract only ϕ_{defo} term and other terms are either corrected for or treated as noise. In radar interferometry surface deformation studies, the topographic signal must be removed from the flattened interferometric phase to isolate the surface deformation contribution. This technique is called "Differential Interferometry" or D-InSAR. This was first successfully applied to study the Landers earthquake (Massonnet et al., 1993; Zebker et al., 1994). There are four general approaches for the elimination of topography in radar interferometric applications:

1. The minimization of the perpendicular baseline component
2. The two-pass technique,
3. The three-pass technique and
4. The four-pass technique.

The minimization of the perpendicular baseline component for topographic elimination amounts to selecting interferometric pairs for which the perpendicular baseline component is sufficiently small as to assume the topographic component is negligible. When possible, this technique is preferred as it avoids the introduction of topographic measurement errors and significant increases in computational loads.

In a two-pass method, a digital elevation model (DEM) such as from the Shuttle Radar Topography Mission (SRTM) (Farr et al., 2007) or another interferogram (Gabriel et al., 1989) of the same area can be used to estimate the ϕ_{topo} term. The slightly different imaging geometries also produce a slight parallax, if the area has topography. The Two-pass method uses an external elevation model that is converted into radar coordinates, scaled using the baseline, and subtracted from the interferogram (Massonnet et al., 1993). This can be a feasible approach, as elevation models are available for many areas in the world. With the release of 1-arc second SRTM data, this approach is gaining popularity in the field of deformation study of land due to earthquake event. The major disadvantage of this approach is that errors in DEM will propagate into the deformation results. Also, it is not always possible to find a DEM of the area and sometimes the exact datum of the DEM may be unknown (Rosen and Hansley, 1996). This technique requires the DEM to be mapped into radar coordinates (interferogram simulation).

The advantages of two-pass technique are: (1) The phase unwrapping of a topography interferogram with significant phase variations is not required, (2) Geolocation does not depend on the quality of the unwrapped topography interferogram and (3) Geolocation is a by-product of DEM simulation process,

A second method called as three-pass method (Zebker et al., 1994). In this method an extra SAR acquisition is used and combined with an appropriate image acquisition to create the so-called topographic pair as shown in Figure 4.

The pair is assumed to have no deformation, a suitable baseline providing sensitivity to topography, and sufficient coherence. This pair is unwrapped, scaled to the baseline characteristics of the deformation pair and subtracted from it yielding the differential interferogram.

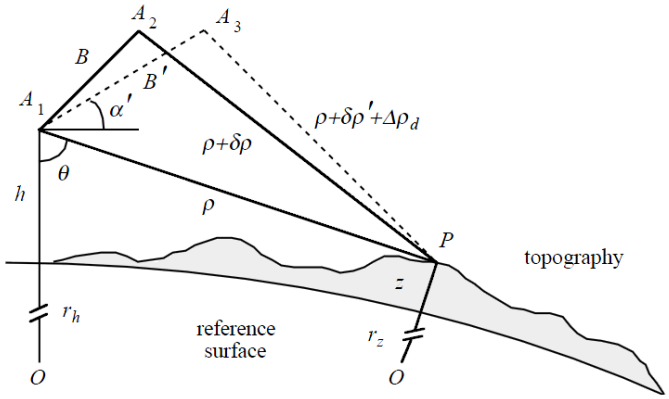

Figure 4: Three-pass Geometry

(Source: Buckley, 2000)

In order to perform the three-pass method, using a topographic pair, the effect of the baseline difference between the two pairs should be taken into account. The baseline can be scaled after the reference phase is subtracted from both interferograms. The major problem with the three-pass method is the availability of suitable image pairs. Since the topography-only interferometric phase is scaled before being subtracted from the topography and deformation interferometric phase, the phase associated with the topography-only interferogram must be unwrapped. The phase unwrapping errors can introduce deformation errors and complications in the geo-location process. The advantages of three-pass method are (1) in remote locations, where DEM may not be available, the radar acquisitions may be used for the measurements, (2) Errors due to DEM i.e. height errors in the external DEM can be avoided and (3) since radar images are in radar coordinates, computational loads are eased and interpolation errors are avoided that are associated with DEM simulation.

For the three-pass method to be applied, one common image has to be used for both the topographic pair and the deformation pair. The common image is then used as a reference to align the other two. Due to the available baselines for a specific scene, it may happen that the common image is not available. For example, the baselines for all the available image pairs of the deformation pair are too large, reducing coherence in the topographic pair and hampering phase unwrapping. In that case, the four-pass method can be used, where the topographic pair and the deformation pair are independent, i.e. they share no common SAR acquisition. Figure 5 shows the geometry of four-pass method.

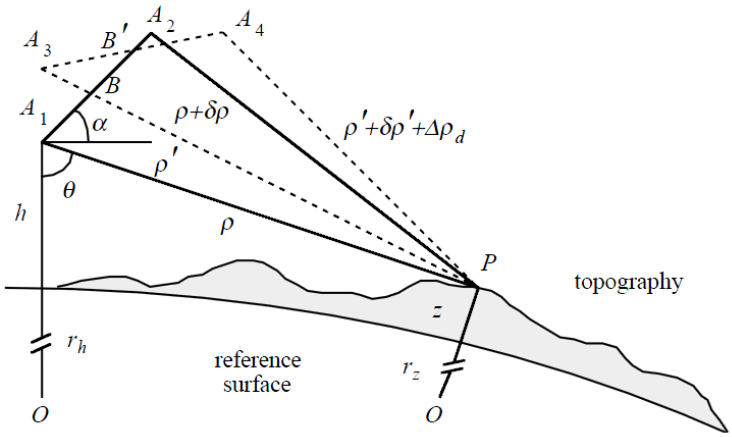

Figure 5: Four pass Geometry

(Source: Buckley, 2000)

The difference between the four-pass and three-pass methods is that in the four-pass method the influence of atmospheric signal will be more and in the co-registration of the images. Differential interferogram generation requires the two interferograms (the deformation pair and the topographic pair) to be aligned to the same grid. In three-pass differential interferometry this requirement is satisfied by using a common reference image, onto which the other two are coregistered and resampled. The four pass technique requires a repeated co-registration and interpolation. First the two interferograms are formed separately, followed by the coregistration of one of the pairs onto the other. After all images are in the same grid, the topographic pair needs to be unwrapped and scaled according to the baseline ratio between the two interferograms. Subtracting this unwrapped, scaled topographic pair from the deformation pair yields the differential pair, which should ideally reflect only deformation signal.

In addition to the three-pass technique,(sentence needs to be changed)the four-pass method is easier to implement as it is not always possible to find three-pairs with the same common

image for the two interferograms (topographic and deformation pair). The disadvantages associated with the four-pass method are same as of the three-pass method. The additional disadvantage of the four-pass method is the requirement of the additional to process the fourth image and resample one interferogram to another.

For the study of long term deformation, advanced DInSAR tecniques like Persistent Scatterers Interferometry (PSI) technique. Subsequent to the development of the PSI technique which was started with the so-called Permanent Scatterer technique proposed by Ferretti et al.(2000), several other related approaches were developed and proposed ((Ferretti et al. (2001), Berardino et al. (2002), Colesanti et al. (2003), Mora et al.(2003), Lanari et al. (2004), Hooper et al. (2004), Kampes and Hanssen (2004), Crosettoet al. (2005), Crosetto et al. (2008a), Hanssen and van Leijen(2008)). Initially, the techniques were referred to as "Permanent Scatterer techniques", but now all of them, including the original Permanent Scatterer technique, are usually called "PSI techniques". The term "Permanent Scatterers" is exclusively associated with the original technique patented by Ferretti et al.

4.0 Methodology and Results

Two-Pass differential interferometric technique was used in this study. Following are the steps of the two-pass technique.

1. Interferogram generation

Using the SLCs of the pre and post-earthquake data, interferogram is generated. Figure 6 shows the generated interferogram with 24th May 2015 as the master image (pre-earthquake) and 6th May 2015 (post-earthquake) as the slave image. It is generated by multiplying the master image with the complex conjugate of the slave image. The interferogram generated contains the information of phase difference.

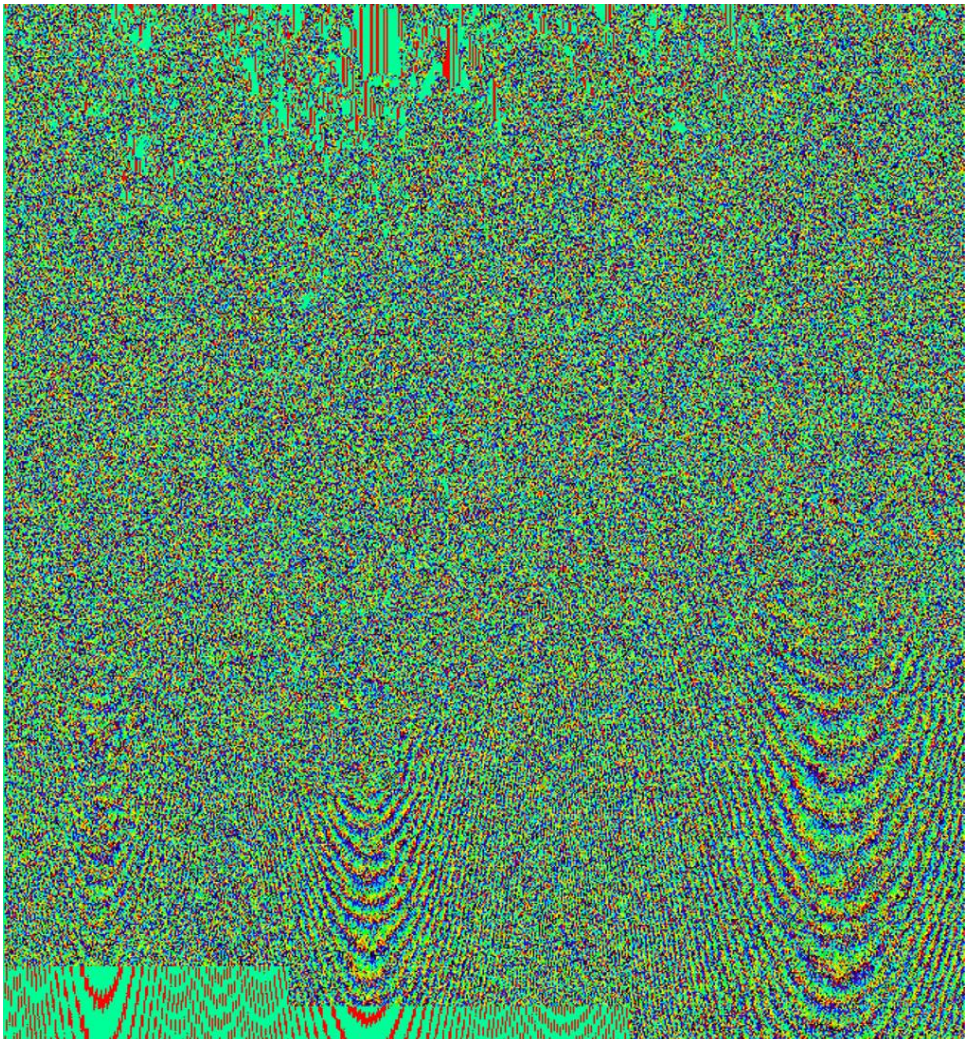

Figure 6: Interferogram generated using 24th April 2015 and 6th may 2015 image of Eastern Nepal

2. Differential Interferogram generation

In order to remove the topography related fringes, external DEM (SRTM 90m DEM) (Figure 7) is used and differential interferogram is generated. The step is necessary so that the phase in the differential interferogram contains only the phase difference information because of the land deformation or movement of the land surface. Figure 8 shows the differential interferogram of the study area. Distinct fringes can be easily seen in the southern part of the interferogram. Also, throughout the interferogram, fringes are visible.

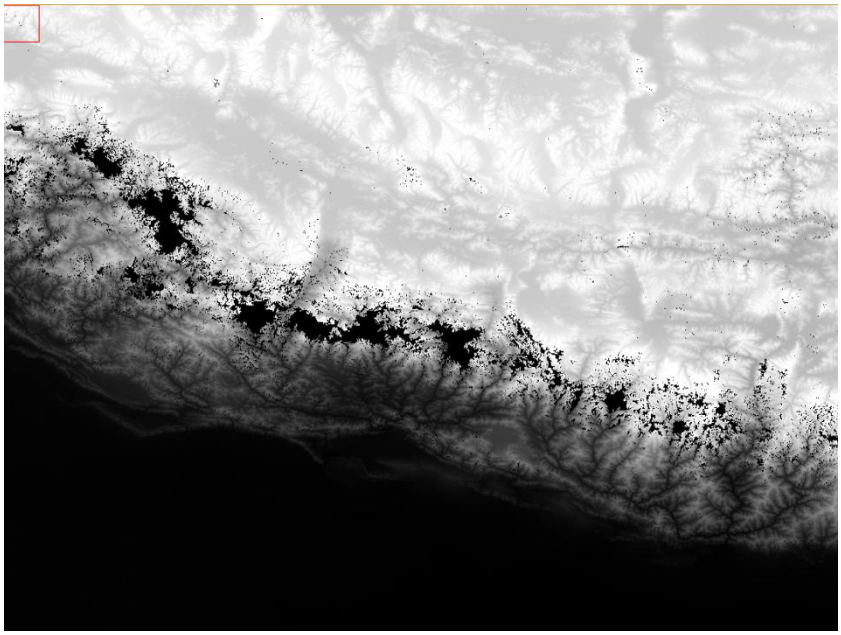

Figure7: 3 arc second SRTM DEM of Nepal and surroundings

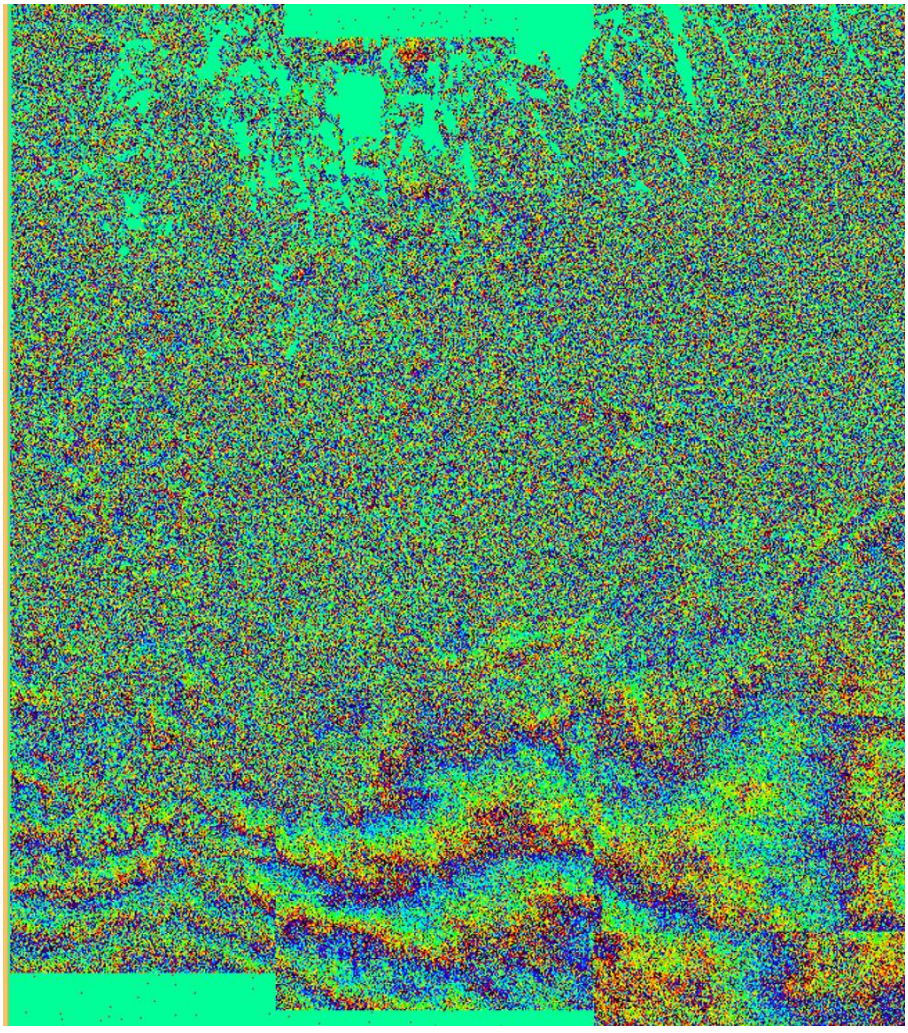

Figure 8: Differential Interferogram generated using SRTM 90 m DEM

3. Adaptive filter and Coherence generation

After generation of the interferogram, adaptive filtering and coherence generation step is performed. Figure 9 show the filtered differential interferogram.

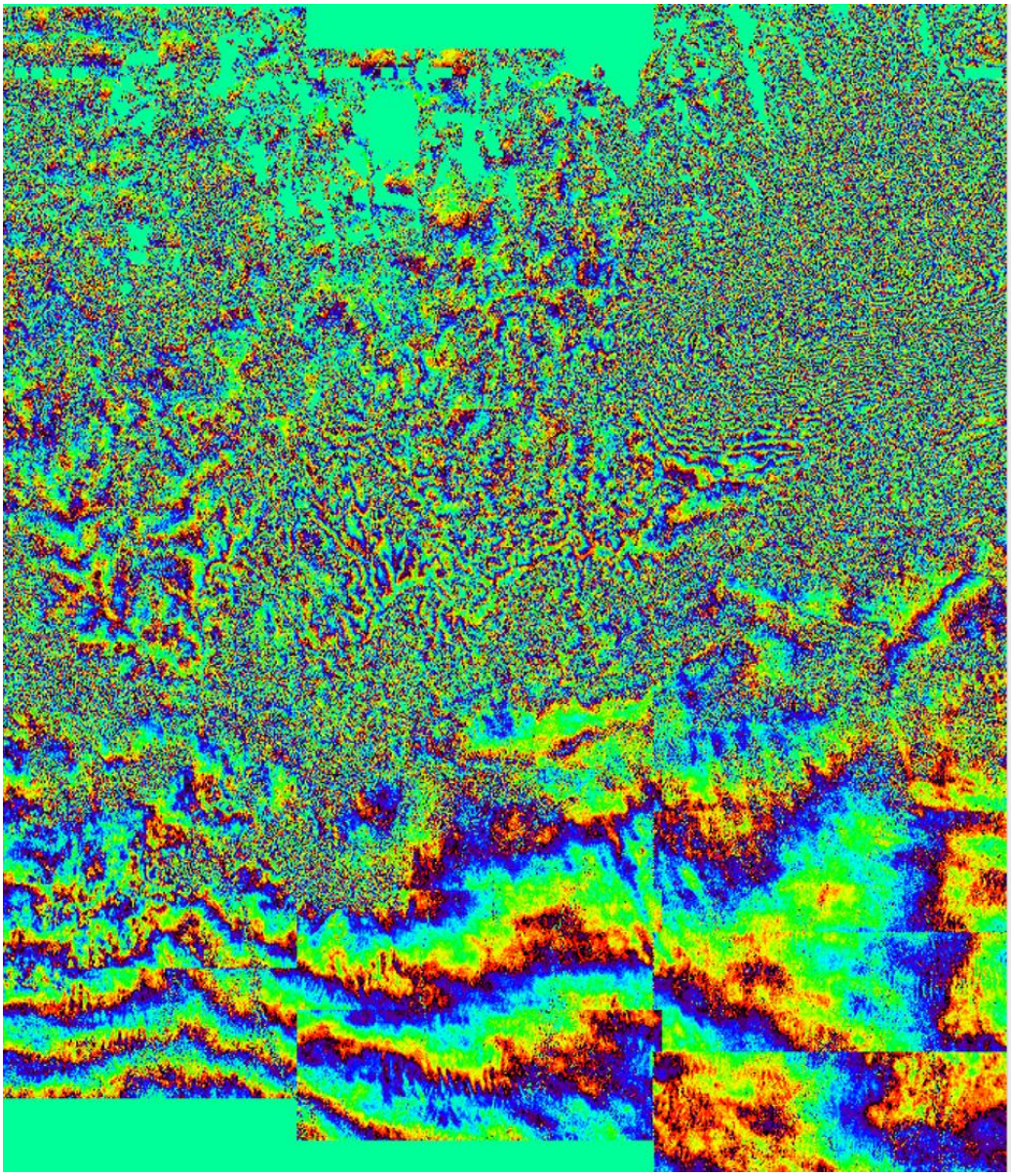

Figure 9: Filtered Differential Interferogram

4. Phase Unwrapping

Filtered interferogram is used as an input to generate the unwrapped phase. The phase of the interferogram can only be modulo 2π; hence anytime the phase change becomes larger than 2π the phase starts again and the cycle repeats itself. Phase Unwrapping is the process that resolves this 2π ambiguity. Several algorithms (such as the branch-

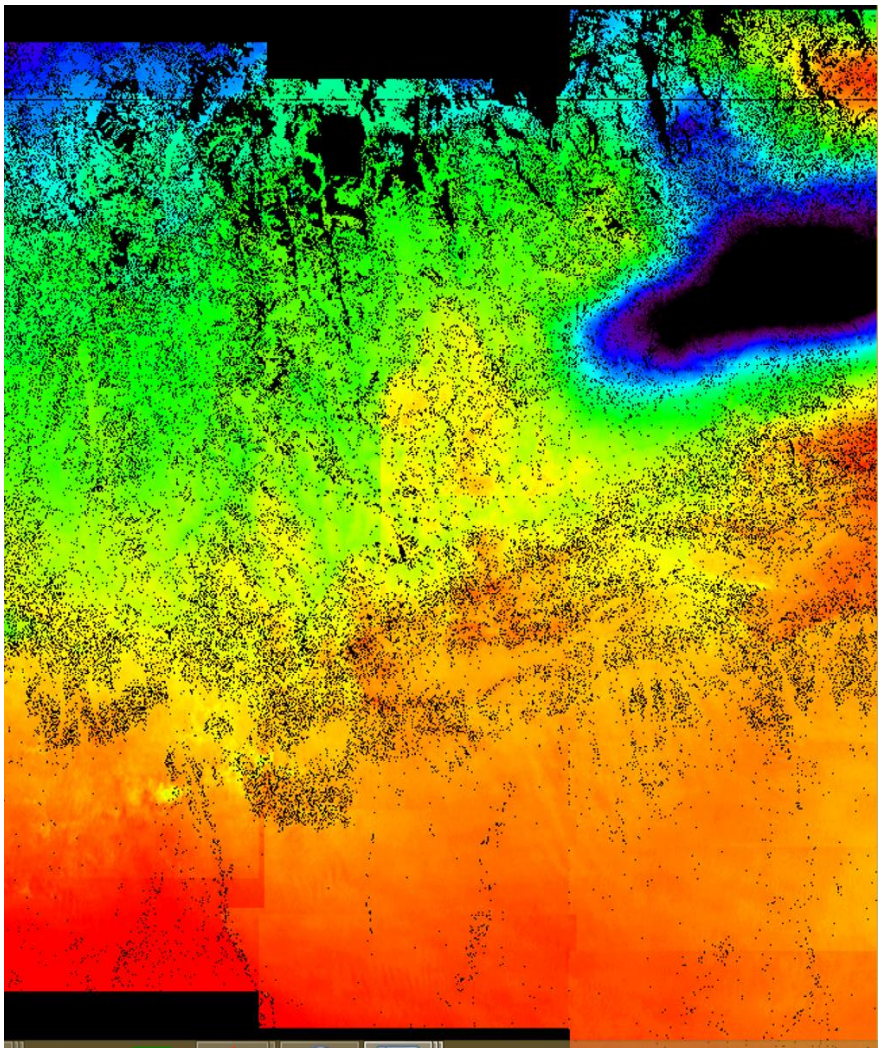

Figure 10 a: Unwrapped Phase

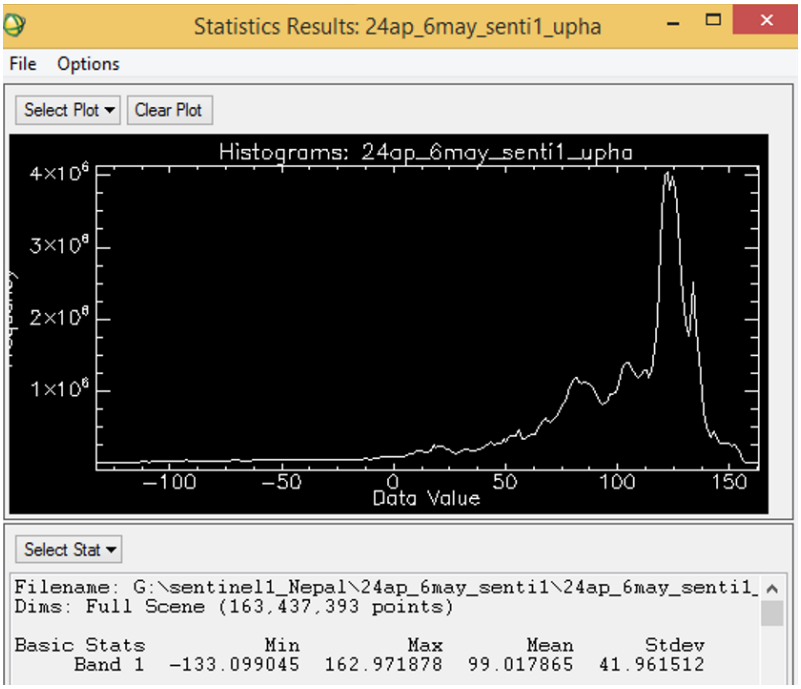

Figure 10 b: Unwrapped Phase statistics

cuts, region growing, minimum cost flow, minimum least squares, multi-baseline, etc.) have been developed; in essence, none of these is perfect and different or combined approaches should be applied on a case by case basis to get optimal results. In this study, minimum cost flow method has been used for phase unwrapping. Figure 10 a and b shows the generated unwrapped phase and its statistics respectively.

5. Refinement and Reflattening

This step is crucial for a correct transformation of the unwrapped phase information into height (or displacement) values. It allows both to refine the orbits (i.e. correcting possible inaccuracies) and to calculate the phase offset (i.e. getting the absolute phase values), or remove possible phase ramps. Figure 11 (a) and (b) shows the reflattened unwrapped phase and corresponding statistics.

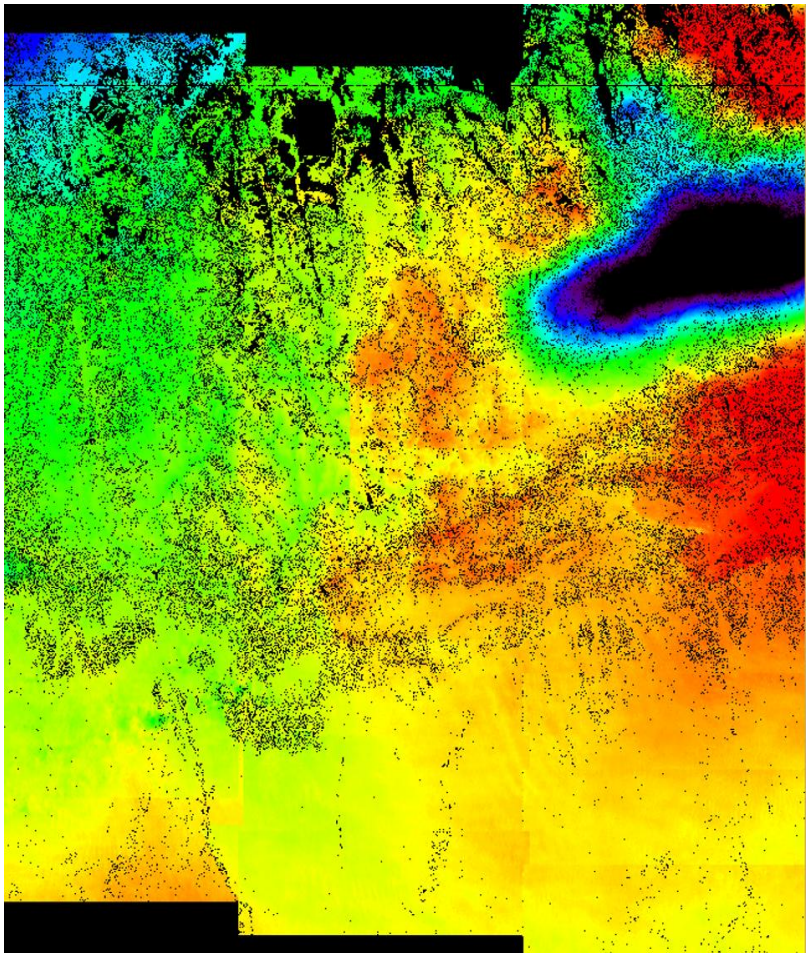

Figure 11 a: Flattened Unwrapped Phase

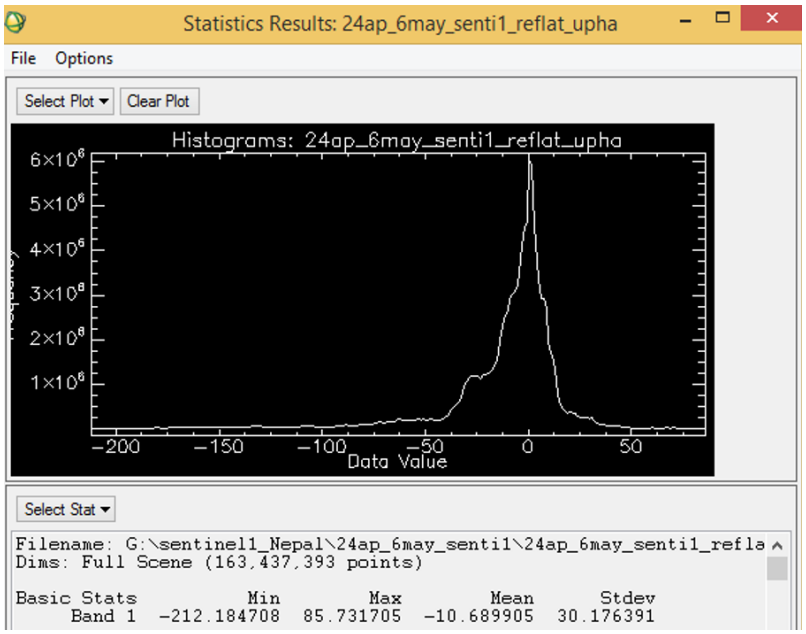

Figure 11 b: Flattened Unwrapped Phase Statistics

6. Phase to displacement conversion and geocoding

The absolute calibrated and unwrapped phase values are converted to displacement and directly geocoded into a map projection. This step is performed in a similar way as in the geocoding procedure (Basic module), by considering the Range-Doppler approach and the related geodetic and cartographic transforms. Each 2π cycle (interferometric fringe) of differential phase corresponds to half wavelength of displacement along the Slant Range direction (SAR viewing direction).

This output product, which is derived from parameters such as coherence and wavelength, provides an estimate (i.e. standard deviation value) of the measurement precision. The higher this value the lower the measurement precision. The formula used for the precision calculation is:

$$\sqrt{\frac{1-\gamma^2}{2\gamma^2}}\ \frac{\lambda}{4\pi}$$

where γ is the interferometric coherence.

Figure 12 (a) and (b) shows the generated land deformation map and corresponding staistics. Figure 12 (c) shows the precision image.

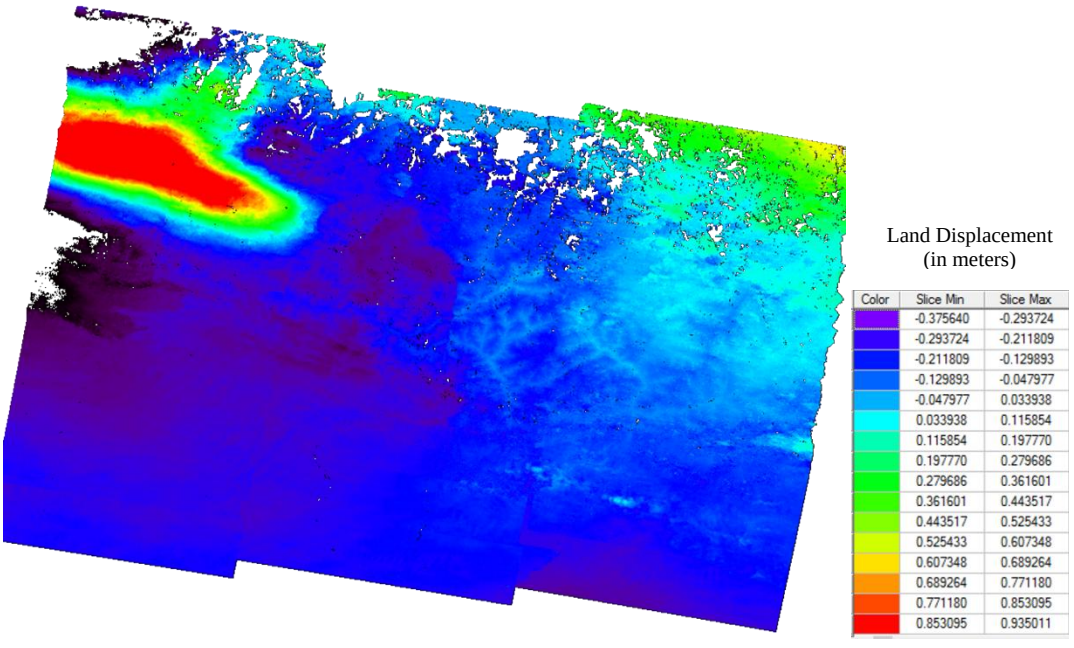

Figure 12 a: Land Deformation Map for Eastern part of Nepal

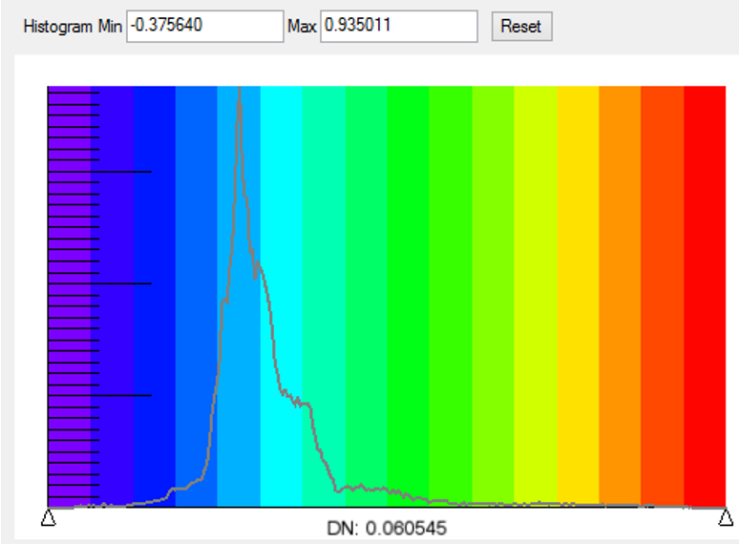

Figure 12 b: Statistics of land displacement

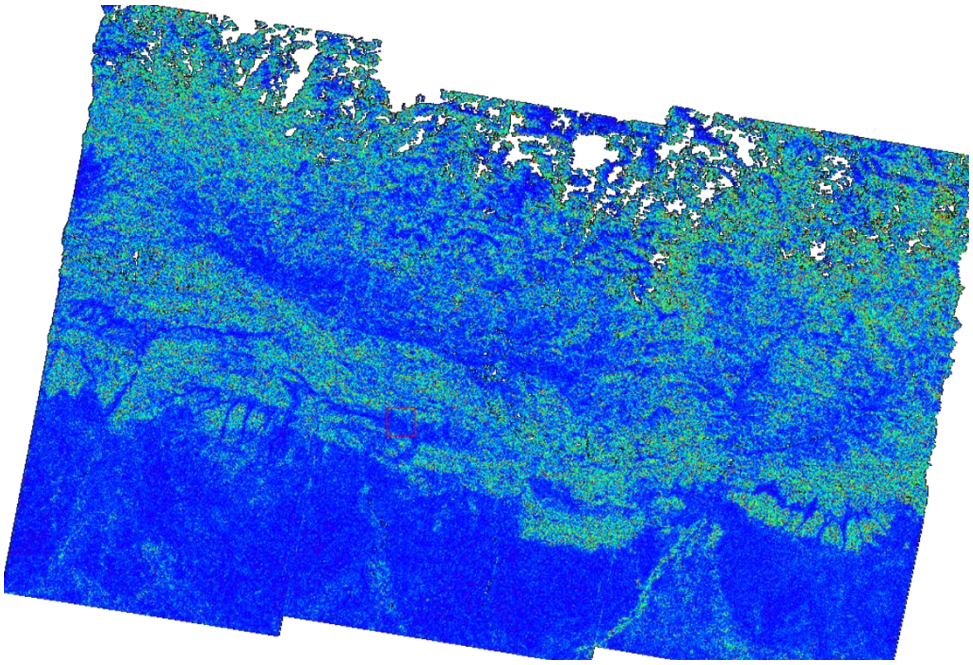

Figure 12 c: Precision Image

In the precision image, the color coding is 'rainbow' with the value gradually increasing from blue to red. The mean value of the precision image is 10.5 cm i.e the mean value of the standard deviation of the measurement precision is 10.5 cm. From figure 12 (c) it can be seen that in the high elevation area (upper part and the middle part) the standard deviation is more as compared to the lower part of the image with lower elevation values. This may be due to the layover and shadow effect.

4.1 Preliminary Results Using SRTM 30 m DEM

For a small part of the eastern Nepal, land deformation map was generated using SRTM 30m DEM. Figure 13 shows the area processed with SRTM 30m DEM.

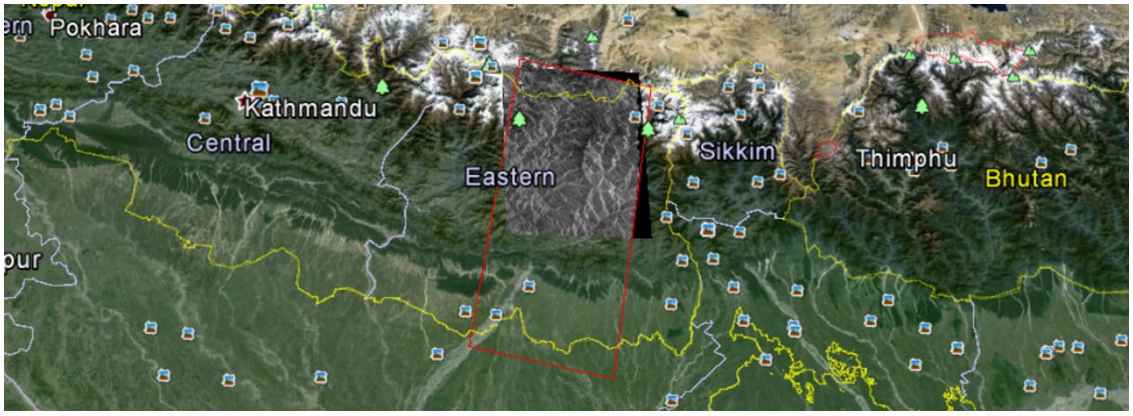

Figure 13: Part of the eastern Nepal processed with SRTM 30m DEM (courtesy: Google Earth)

Using the same methodology as described above, the deformation map was generated. Figure 14 shows a part of filtered interferogram and figure 15 shows the displacement map generated.

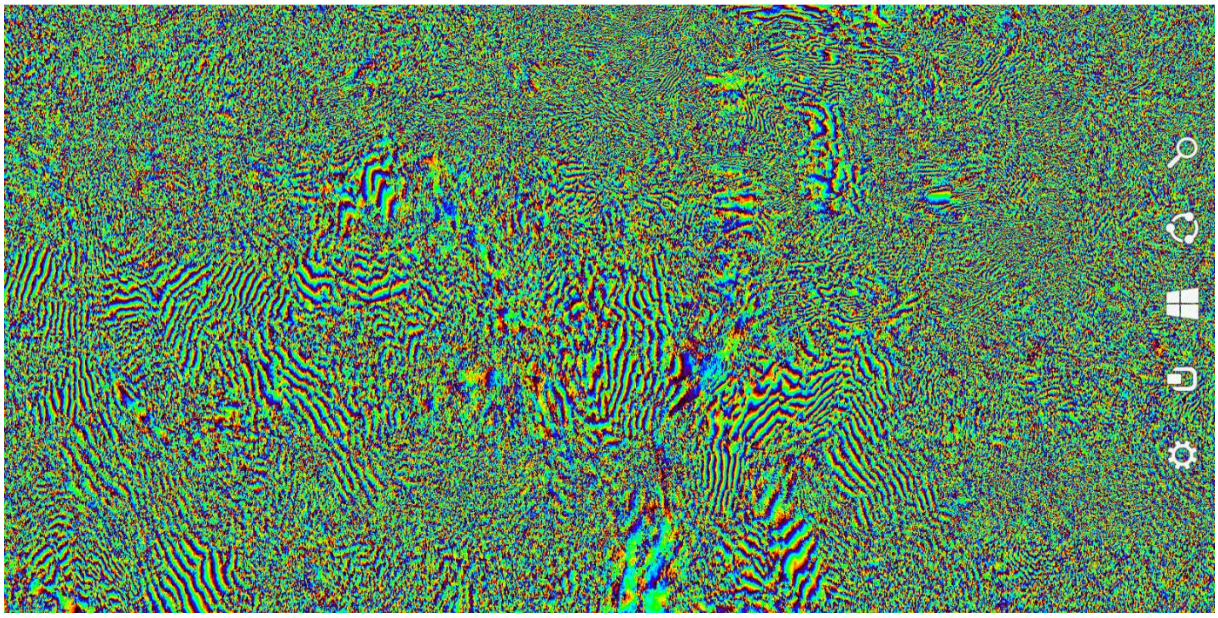

Figure 14: Filtered Interferogram for a part of the Eastern Nepal processed with SRTM 30m DEM

Fringes are seen very clearly in the processed interferogram in figure 14.

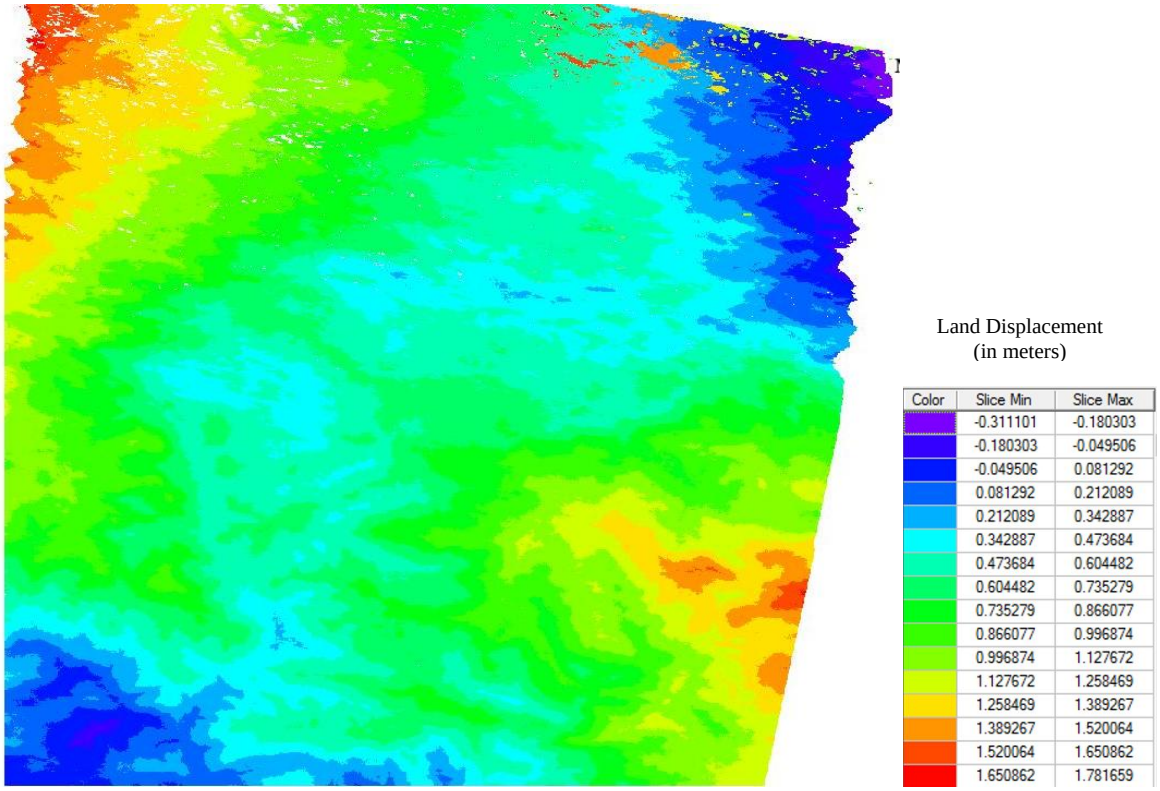

Figure 15: Land Displacement map genearted for a part of the Eastern Nepal processed with SRTM 30m DEM

The mean precision value for displacement map was found to be 22.3 cm which is greater than the map generated using SRTM 90 m DEM. Refinement of the map generated is in progress.

5.0 Conclusions

This work carries out the mapping of land displacement due to Gorkha earthquake in Nepal on 25th April 2015. Land displacement map was generated for eastern part of Nepal using Sentinel-1 IW-SLC, VV data using two-pass differential interferometry technique and SRTM 90 m DEM. It was found that the slant range displacement was in the range of -37.5 to 93.5 cm. The part near to Kathmandu showed upliftment with maximum value close to 1 m, whereas the lower part of the area showed subsidence. For a small part of the far eastern Nepal, displacement map was generated using 1 arc second SRTM DEM and it showed the slant range displacement in the range of -31.1 cm to ~2m.

6.0 Future Work

Following studies are planned in the future:

1. Generation of displacement map for the second earthquake that hit on 12th May 2015 using SRTM 90m and 30m DEM.
2. Generation of displacement map using three pass method.

Acknowledgements

The authors would like to express their gratitude and sincere thanks to Director SAC, Sri Tapan Misra for the constant encouragement and support. We owe our sincere thanks to Dr. B.S. Gohil, Group Director, MPSG, Space Applications Centre, Ahmedabad, for his continuous support and for his comments and suggestions. We are also grateful to European Space Agency (ESA) for providing Sentinel-1 data for the study.

References:

Bilham Roger and Michael Jackson,"Constraints on Himalayan Deformation inferred from Vertical Velocity Fields in Nepal and Tibet," Journal of Geophysical Research, vol. 99, 897–912, 10 July 1994.

Blanco, P., Mallorqui, J., Duque, S. and Monells, D., "The coherent pixels technique (CPT): An advanced DInSAR technique for nonlinear deformation monitoring", Pure and Applied Geophysics, 165(6): 1167-1193, 2008.

Buckley M.S., "Radar interferometry measurement of land subsidence", Dissertation report, The University of Texas at Austin, August 2000, http://adsabs.harvard.edu/abs/2000PhDT.....293B.

Calò, F. (2012). Doris Project: The European Downstream Service Forlandslides andSubsidence Risk Management. Geoscience and Remote Sensing Symposium(IGARSS), 2012 IEEE International (pp. 3018 – 3021). Naples, Italy, 22-27 July2012.

Canova, F., Tolomei, C., Salvi, S., Toscani, G., & Seno, S., " Land subsidencealong the Ionian coast of SE Sicily (Italy), detection and analysis via SmallBaseline Subset (SBAS) multitemporal differential SAR interferometry", EarthSurface Processes and Landforms, 37(3), 273–286, 2012.

Casu, F., Manzo, M., & Lanari, R. (2006a).A quantitative assessment of the SBASalgorithm performance for surface deformation retrieval from DInSAR data.Remote Sensing of Environment, 102(3-4), 195–210.

Cascini, L., Fornaro, G., & Peduto, D.,"Advanced low- and full-resolutionDInSAR map generation for slow-moving landslide analysis at different scales", Engineering Geology, 112(1-4), 29–42, 2010.

Chang, C.P., Wang, C.T., Chang, T.Y., Chen, K.S., Liang, L.S., Pathier, E., andAngelier, J., "Application of SAR interferometry to a large thrustdeformation: the 1999 M-w=7.6 Chichi earthquake in central Taiwan", Geophysical Journal International, v. 159, pp: 9-16, 2004.

Chang, H.C., "Differential Interferometric Synthetic Aperture Radar for LandDeformation Monitoring", PhD Thesis, School of Surveying and Spatial Information Systems, University of New South Wales, 183pp,2008.

Colesanti, C., Ferretti, A., Locatelli, R. and Savio, G., "Multi-platform permanent scatterers analysis: first results", In: Second GRSS/ISPRS Joint Workshop on "Data Fusion and Remote Sensing over Urban Areas, Berlin, Germany, 22 – 23 May: 52-56, 2003a.

Colesanti, C., Ferretti, A., Novali, F., Prati, C. and Rocca, F., "SAR monitoring of progressive and seasonal ground deformation using the permanent scatterers technique", IEEE Transactions on Geoscience and Remote Sensing, 41(7): 1685-1701, 2003b.

Colesanti, C., Locatelli, R. and Novali, F., "Ground deformation monitoring exploiting SAR permanent scatterers", In: IGARSS 2002, Toronto, Canada, 24-28 June: 203-207 vol.1, 2002.

Crosetto, M., Crippa, B., Biescas, E., “Early detection andin-depth analysis of deformation phenomena by radarinterferometry”, Engineering Geology, 2005.

Crosetto, M., Bremmer, C., Hanssen, R., Capes, R., and Marsh, S., “Groundmotion monitoring using SAR interferometry: Quality assessment”, *EuropeanGeologist*, 12–15, 2008.

D. Massonnet, M. Rossi, C. Carmona, F.Adragna, G. Peltzer, K. Feigl, T. Rabaute, “TheDisplacement Field of the Landers Earthquake Mapped byRadar Interferometry”, Nature, 364**,** 1993.

D. A. Schmidt and R. Bürgmann, “Time-dependent land uplift and subsidencein the santaclara valley, california, from a large interferometricsynthetic aperture radar data set,” *J. Geophys.Res.*, vol. 108, no. B9,pp. 1–13, 2003.

Dominguez, J., Romero, R., Carrasco, D., Martinez, A., Mallorqui, J.J., Blanco, P. and Navarrete, D., “Advanced DInSAR based on coherent pixels: Development and results using CPT technique”, In: Proceedings of the FRINGE 2005Workshop, Frascatti, Italy, 28 November - 2 December: 11.1, 2005.

Duro, J., Inglada, J., Closa, J., Adam, N. and Arnaud, A., “High resolution differential interferometry using time series of ERS and Envisat SAR data” In Proceedings of the 2004 Envisat& ERS Symposium, Salzburg, Austria, 6-10 September: 2P11_4 1-5, 2004.

E. J. Price and D. T. Sandwell, “Small-scale deformations associatedwith the 1992, Landers, California, earthquake mapped by syntheticaperture radar interferometry phase gradients,” *J. Geophys. Res.*, vol.103, pp. 27001–27016, 1998.

Fan, J., Zhao, H., Tu, P., Wang, Y., Guo, X., Ge, D., & Liu, G. , “CRInSAR forlandslide deformation monitoring: A case in threegorge area”, IEEE, IGARSSInternational Geoscience and Remote Sensing Symposium Honolulu, Hawaii,U.S.A (pp. 3956–3959), 2010.

Farr., T.G., Rosen, P.A., Caro, E., Crippen, R., Duren, R., Hensley, S., Kobrick, M. Paller, M., Rodriguez, E. , Roth, L. and others, “The Shuttle radar topography mission”, Reviews of Geophysics, 45 (2), pp: RG2004, 2007.

Farina, P., Colombo, D., Fumagalli, A., Marks, F. and Moretti, S., “Permanent scatterers for landslide investigations: Outcomes from the ESA-SLAM project”, Engineering Geology, 88(3-4): 200-217, 2006.

Ferretti, A., Prati, C. and Rocca, F., “Nonlinear subsidence rate estimation using permanent scatterers in differential SAR interferometry”, IEEE Transactions on Geoscience and Remote Sensing, 38(5): 2202-2212, 2000.

Ferretti, C. Prati, F. Rocca, “Permanent Scatterers in SAR Interferometry”, IEEE Trans. on Geosc. and Rem. Sens., Vol. 39, No. 1, 2001.

Ferretti, C. Prati, F. Rocca, “Non-linear subsidence rate estimation using permanent scatterers in Differential SAR Interferometry”, IEEE Trans. on Geosc.and Rem. Sens, Vol. 38, No. 5, 2000.

Ferreti et al., “A new algorithm for processing interferometric data stacks: SqueeSAR”, IEEE transactions on Geoscience and Remote Sensing, Vol. 49, No.9, September 2011.

Ferretti, A., A. Fumagalli, F. Novali, C. Prati, F. Rocca, and A. Rucci, , “The SecondGeneration PSInSAR Approach: SqueeSAR”, presented at the Fringe Conf., Frascati,Italy, 2009.

Fu, L. L., and Holt, B., “Seasat view oceans and sea ice with synthetic aperture radar”, Tech. rept. Jet Propulsion Lab, 1982.

Gabriel, A.K., Goldstein, R.M. and Zebker, H.A., “Mapping small elevation changes over large areas: Differential radar interferometry”, Journal of Geophysical Research94(B7): 9183-9191, 1989.

H. A. Zebker, J. Villasenor, “Decorrelation inInterferometric Radar Echoes”, IEEE Trans. on Geosc. AndRem. Sens., Vol. 30, No. 5, 1992.

Hanssen, R.F., Radar Interferometry: Data Interpretation and error analysis, kluwer Academic, Dordrecht, 2001.

Hanssen, R., “Atmospheric Heterogeneties in ERS Tandem SAR Interferometry”, Delft University Press, Delft, The Netherlands, 1998.

Herrera, G., Tomás, R., Lopez-Sanchez, J. M., Delgado, J., Vicente, F., Mulas, J.,Cooksley, G., et al., “Validation and comparison of Advanced DifferentialInterferometry Techniques: Murcia metropolitan area case study”, ISPRS Journal ofPhotogrammetry and Remote Sensing, 64(5), 501–512, 2009.

Hooper, A., Zebker, H., Segall, P., and Kampes, B., “A new method for measuringdeformation on volcanoes and other natural terrains using InSAR persistentscatterers”, Geophys. Res. Lett., **31**, L23611, 2004.

Hooper, A.J., “Persistent Scatterer Radar Interferometry for Crustal DeformationStudies and Modelling of Volcanic Deformation*”,* PhD Thesis, Department of Geophysics, Stanford University, USA, 124pp, 2006.

Hooper A., “A multi-temporal InSAR method incorporating both persistent scatterer and small baseline approaches,” Geophys. Res. Lett., vol. 35, no. L16302, pp. 1–5, 2008.

Humme, A., Point Density Optimization for SAR Interferometry; a study Tested on Salt Mine Areas, Master’s thesis, Delft university of Technology, 2007.

Hyvärinen A. and E. Oja."Independent Component Analysis: Algorithms and Applications", Neural Networks, 13(4-5), 411-430, (2000).

Kampes, B. and Hanssen, R.F., "Ambiguity resolution for permanent scatterer interferometry", IEEE Transactions on Geoscience and Remote Sensing, 42(11): 2446-2453, 2004.

Kampes, B. and Nico, A., "The STUN algorithm for persistent scatterer interferometry" In: Proceedings of the FRINGE Workshop 2005, Frascatti, Italy, 28 November - 2 December: 16.1, 2005.

Kampes, B.M, "Radar Interferometry: Persistent Scatterer Technique*",* Springer, Dordrecht, 211 pp., 2006.

Kampes, B.M. and Adam, N., "Velocity field retrieval from long term coherent points in radar interferometric stacks", In: IGARSS 2003, Toulouse, France, 21-25 July: 941-943 vol.2, 2003.

Lanari, R., Zeni, G., Manuta, M., Guarino, S., Berardino, P., and Sansosti, E., " An integrated SAR/GIS approach for investigating urban deformationphenomena: a case study of the city of Napoli, Italy",International Journal of Remote Sensing, **25**(14), 2855–2867,2004a.

Lanari, R., Mora, O., Manunta, M., Mallorqui, J. J., Berardino, P., and Sansosti, E., " A small-baseline approach for investigating deformations on full-resolution differential SAR interferograms",grs, **42**(7), 1377–1386, 2004b.

Lanari, R., F. Casu, M. Manzo, G. Zeni, P. Berardino, M. Manunta, and A. Pepe, An Overview of the Small Baseline Subset Algorithm: A DInSAR Technique for Surface Deformation Analysis, Pure and Applied Geophysics, 164(4), 637–661, 2007.

Laur H., P. Bally, P. Meadows, J. Sanchez, B. Schättler, E.Lopinto and D. Esteban.,"Derivation of the BackscatteringCoefficient σ0 in ERS SAR PRI Products", Document No. ESTN-RS-PM-HL09, http://earth.esa.int/ESC2, 2002.

Marghany, M., " Three-dimensional visualisation of coastal geomorphology usingfuzzy B-spline of dinsar technique", International Journal of the Physical Sciences,6(30), 6967–6971, 2011.

Meisina, C., Zucca, F., Fossati, D., Ceriani, M., & Allievi, J.,"Grounddeformation monitoring by using the Permanent Scatterers Technique: Theexample of the Oltrepo Pavese (Lombardia, Italy)", Engineering Geology, 88(3-4),240–259, 2006.

Nepal quake 'followed historic pattern'". BBC. April 27, 2015.

NPA, "Wraysbury Reservoir - Monitoring of Reservoir Loading using CRInSAR*",* Nigel Press Associates. Available from: http://www.npagroup.co.uk/insar/apps/wraysbury_reservoir_crinsar.htm, 2009.

O. Mora, J. J. Mallorqu´ı, and A. Broquetas, "Linear and nonlinear terrain deformation maps from a reduced set of interferometric SAR images," IEEE Transactions on Geoscience and Remote Sensing, Vol. 41, No. 10, pp. 2243–2253, 2003.

Onn, F., and Zebker, H. A., " Correction for interferometric syntheticaperture radar atmospheric phase artifacts using time series of zenith wet delay observations from a GPS network"J. Geophys. Res,**111**(B09102), 2006.

Osmanoglu, Batuhan, "Applications and Development of New Algorithms for Displacement Analysis Using InSAR Time Series".Open Access Dissertations, Paper 622,2011.

Parizzi, A., and R. Brcic, Adaptive InSAR Stack Multilooking Exploiting AmplitudeStatistics: A Comparison Between Different Techniques and Practical Results,Geoscience and Remote Sensing Letters, IEEE, (99), 441–445, 2011.

Pandey M.R, R.P. Tandukar, J.P. Avouac, J. Vergne and Th. Heritier, "Seismotectonics of the Nepal Himalaya from a Local Seismic Network", Journal of Asian Earth Sciences,17, 703–712,1999.

P. A. Rosen, S. Hensley, H. A. Zebker, F. H.Webb, and E. J. Fielding,"Surface deformation and coherence measurements of Kilauea Volcano,Hawaii, from SIR-C radar interferometry," *J. Geophys. Res.*,vol. 268, pp. 1333–1336, 1996.

PiyushShankerAgram, "Persistent Scatterer Interferometry in natural terrain", a dissertation, Auguat 2010, www.stanford.edu/group/radar/people/piyush_thesis_small.pdf.

P.M. Balaji, "Estimation and correction of tropospheric and ionospheric effects on differential SAR interferogram", a thesis, Netherlands, April, 2011, www.itc.nl/library/papers_2011/msc/gfm/balaji.pdf.

Qi-huan, H., & Xiu-feng, H. (2008). Surface deformation investigated with sbas-dinsarapproach based on prior knowledge. The International Archives of thePhotogrammetry, Remote Sensing and Spatial Information Sciences, XXXVII(1).

Raucoules D., Colesanti C and Carnec C., (2007), Üse of SAR interferometry for detecting and assessing ground subsidence", Comptes Rendus geosciences, vol. 339, no. 5, pp 289-302, 2007.

R. F. Hanssen, "Radar Interferometry. DataInterpretation and Error Analysis", Dordrecht, KluwerAcademic Publishers, 2001.

Richman D.,"Three dimensional azimuth-correcting mapping radar", United Technologies Corporation, USA, 1971.

Rosen et al., "Synthetic Aperture radar Interferometry", invited paper in Proceedings of the IEEE, vol. 88, No.3, March 2000.

R. M. Goldstein, H. A. Zebker, and C. L.Werner, "Satellite radar interferometry:Two-dimensional phase unwrapping," *Radio Sci.*, vol.23, no. 4, pp. 713–720, July/Aug. 1988.

Seymour, M.S. and Cumming, I.G., "Maximum likelihood estimation for SAR interferometry", In: IGARSS 1994, Pasadena, CA, USA, 8 - 12 August: 2272-2275, 1994.

S. Usai, “A least squares database approach for SAR interferometric data,” IEEE Transactions onGeoscience and Remote Sensing, Vol. 41, No. 4, pp. 753–760, 2003.

Sousa, J., A. Hooper, R. Hanssen, and L. Bastos, “Comparative Study of Two DifferentPS-INSAR Approaches: DEPSI vs. STAMPS”, in ESA Fringe Workshop 2009.

Tarikhi, P. 2010,“Radar DEM generation_; achievements and benefits”,Wordpress.com. Retrieved fromhttp://parviztarikhi.wordpress.com

Tarikhi, P.,“InSAR New generation”, Position Magazine, Australia:November/December 2011. Issue 50, p42 – 44, 2011.

Tarikhi, P.,“Liqui-InSAR; SAR Interferometry for aquatic bodies”, Wordpress.com. http://parviztarikhi.wordpress.com, 2012.

Usai S. and R. Hanssen, “Long time-scale InSAR by means of high coherence features”, European Space Agency Special Publication ESA SP-414, Proc. 3rd ERS symposium, 17-21 March, 1997, Florence, Italy, 225-28, 1997.

Van der Kooij, M., Hughes, W., Sato, S. and Poncos, V., “Coherent target monitoring at high spatial density, examples of validation results”, In: Proceedings of the FRINGE Workshop 2005,Frascati, Italy, 28 November - 2December: http://earth.esa.int/workshops/fringe2005/proceedings/ 2005.

Van der Kooij, M. and Lambert, A., “Results of processing and analysis of large volumes of repeat-pass InSAR data of Vancouver and Mount Meager (B.C.)” In: IGARSS 2002, Toronto, Canada, 24-28 June: 1228-1230, 2002.

Web1: http://www.icc.es/cat/Media/Files/DInSAR-Techniques-versus-High-Topographic-Leveling-Surveys-The-Subsidence-Phenomena-in-Sallent
Last accessed on 19th May2015

Web2: www.isprs.org/proceedings/XXXV/congress/comm7/papers/123.pdf
Last accessed on 19th May2015

Werner, C, Strozzi, T., & Wiesmann, A.,“ERS – ASAR Integration in theInterferometric Point Target analysis”, Fringe ATSR Workshop 2005_: Advances inSAR Interferometry from ENVISAT and ERS missions (pp. 1–6). Frascati, Italy, 28.Nov. – 2. Dec. 2005.

Werner, C., Wegmuller, U., Strozzi, T. and Wiesmann, A., “Interferometric point target analysis for deformation mapping” In: IGARSS 2003, Toulouse, France, 21-25 July: 4362-4364 vol.7, 2003.

Warren, M.A., “The Development of a 3-Pass Persistent Scatterer Algorithm Using the Integer Ambiguity Search Method”., PhD Thesis, Institute of Engineering Surveying and Space Geodesy, School of Civil Engineering, University of Nottingham, UK, 233pp, 2007.

Zebker H. A., Werner, C. L., Rosen, P.A. and Hensley, S., "Accuracy of topographic maps derived from ERS-1 interferometric radar", IEEE transcations on Geosciences and Remote Sensing, 32 (40, pp: 823-836, 1994.

Zisk, S., Lunar topography: first radar-interferometer measurements of the Alphonsus-Ptolemaeus-Arzachel region, *Science, 178,* 977-980, 1972a.

Zisk, S., A new Earth-based radar technique for the measurement of lunar topography,*Moon, 4*, 296-306, 1972b.